RSC Advances

PAPER

View Article Online
View Journal | View Issue

Cite this: *RSC Adv.*, 2024, **14**, 33774

Synthesis, characterization, and antibacterial study of chitosan–zinc oxide nanocomposite-coated superhydrophobic cotton fabric†

Kranti S. Kachare,[a] Shital S. Shendage,[a] Shirishkumar B. Vhanbatte,[b] Fu D. Mai[c] and Anil Vithal Ghule*[a]

Awareness of microbial infection, hygiene, and personal health has increased in recent years, particularly in light of the pervasive pandemic encountered by the global community. This has prompted the development of antibacterial and superhydrophobic cotton fabric to address the pressing challenge. In this investigation, we report bio-mediated zinc oxide nanoparticles (ZnO NPs) synthesized using *Psidium guajava* leaf extract and zinc acetate. Further, the chitosan–ZnO nanocomposite (CS–ZnO) was synthesized and subsequently deposited on cotton fabric (CF) *via* a facile and cost-effective pad-dry-cure method to produce CS–ZnO-CF. The ZnO NPs, CS–ZnO, and CS–ZnO CF were characterized using FTIR, XRD, SEM-EDAX, TGA and AFM analysis. Additionally, we investigated the mechanical properties and water contact angle (WCA) of uncoated cotton (UCF) and CS–ZnO CF. The CS–ZnO-CF demonstrated good mechanical stability even after 50 abrasion cycles, good washing durability, and good super-hydrophobicity, with a high WCA (153.1°). The antibacterial study indicated that CS–ZnO and CS–ZnO-CF exhibited higher antibacterial activity than UCF against *Escherichia coli* (*E. coli*) and *Staphylococcus aureus* (*S. aureus*) bacteria. This study introduces a simple, environmentally friendly, and economically scalable method for producing multifunctional CS–ZnO CF, showcasing its potential for diverse applications.

Received 16th August 2024
Accepted 4th October 2024

DOI: 10.1039/d4ra05950f

rsc.li/rsc-advances

1. Introduction

The growing emphasis on personal health and hygiene has led to an increasing demand for developing textiles endowed with antibacterial and hydrophobic properties. Cotton fabrics, widely used in daily life, have a highly hydrophilic nature that tends to retain moisture, creating an environment conducive to the growth and multiplication of various microorganisms. This can result in disease transmission, unpleasant odours, deterioration, and discoloration of textiles.[1] To mitigate these issues, recent efforts have focused on developing multifunctional textiles with promising antibacterial and superhydrophobic properties.[2]

Literature reports indicate that many researchers have sought to develop antibacterial and superhydrophobic coatings on a variety of substrates, including sponges, carbon steel, filter paper, wallpapers, and cotton fabric.[3] Among these, cotton fabric has gained special attention due to its unique characteristics, such as cost-effectiveness, softness, comfort, hygroscopic nature, and biodegradability. Cotton fabric is widely utilized in self-cleaning, UV protection, industrial oil–water separation, decorative uses, and packing.[4] However, in recent years, attention has shifted toward developing either antibacterial or superhydrophobic coatings on cotton fabric, with few studies aiming to achieve a synergistic effect by imparting both properties. Superhydrophobic surfaces, characterized by a water contact angle (WCA) above 150°, can be achieved by coating rough topographical nanostructures with low surface energy materials.[5] For instance, cotton fabric has been treated with various nanoparticles (NPs) such as platinum (Pt), gold (Au), and silver (Ag) to attain effective antibacterial and superhydrophobic properties.[6] Nonetheless, these approaches often come with significant drawbacks, including high costs, poor stability, and limited wash durability, especially when exposed to harsh environmental conditions such as abrasion and washing, which can restrict their commercialization. Alternatively, fluorinated polymers (low surface energy providers) and fluorine-containing modifiers have been widely explored for superhydrophobic coatings. However, these fluoropolymers and fluorine-containing modifiers are likely to cause damage to the environment and the human body.[7,8] Therefore, the main

[a]*Green Nanotechnology Laboratory, Department of Chemistry, Shivaji University, Kolhapur, Maharashtra 416004, India. E-mail: avg_chem@unishivaji.ac.in*
[b]*Textile Physics Laboratory, Dattajirao Kadam Technical Education (DKTE) Society's Textile and Engineering Institute, Ichalkaranji, Maharashtra 416115, India*
[c]*Department of Biochemistry and Molecular Cell Biology, School of Medicine, College of Medicine, Taipei Medical University, Taipei, Taiwan*

† Electronic supplementary information (ESI) available: Fig. S1 XRD pattern of the CS–ZnO nanocomposite. Fig. S2 structure of the CS–ZnO nanocomposite. Fig. S3 TGA thermogram of UCF compared to that of ZnO CF and CS–ZnO CF fabrics. (ZnO loading quantified by comparing the difference in weight loss compared with the UCF). See DOI: https://doi.org/10.1039/d4ra05950f

objective of researchers worldwide is to prepare cost-effective, environmentally friendly, antibacterial and superhydrophobic coatings with improved stability and durability of the coated material, a challenge that is still perceived.

In this context, for integrating both properties, attempts have been focused on developing cost-effective alternatives such as an organic/inorganic hybrid antibacterial nanocomposite. In general, organic antibacterial agents exhibit lower stability at high temperatures and pressure. Conversely, inorganic antibacterial agents are stable, robust, and durable.[9] Thus, a hybrid nanocomposite material was prepared by combining polymers and metal oxide nanoparticles (NPs) with the envisaged improved stability and antibacterial efficiency, which could be attributed to the synergistic effect.[10,11] Among the various polymers explored, chitosan is the polymer of choice in the preparation of the nanocomposite. Chitosan has garnered attention due to its natural abundance, cost-effectiveness, biodegradability, biocompatibility, and nontoxic nature.[12,13] Moreover, chitosan is a linear polysaccharide consisting of D-glucosamine linked by β-(1→4) linkage and *N*-acetyl glucosamine.[14] Apart from this, chitosan acts as a binder in textile finishing, and also as an antibacterial and a surface roughening agent.[13] The role of chitosan as a binder and its high compatibility with cellulose contributes to the high adsorption of NPs onto the fabric surfaces. Thus, the finished fabric exhibits high washing durability. Hence, nanocomposites based on chitosan and metal oxide NPs were used to introduce functional properties into textiles. Among different metal oxides, zinc oxide (ZnO) is an attractive and promising candidate for textile coatings, as it is economical, nontoxic, biocompatible, antibacterial, UV-blocking, and has self-cleaning properties.[15–17] Generally, ZnO NPs are most commonly prepared *via* various chemical and physical approaches, including precipitation, hydrothermal, sol–gel, microwave methods, and thermal decomposition.[18] However, some of these processes require toxic chemicals and high-cost materials and involve multiple time-consuming synthesis steps.[19] In recent years, with an inclination for sustainable development, the green synthesis of ZnO NPs has increasingly attracted interest because of its simple, cost-effective, environmentally friendly, and easy synthesis protocols.[20] In this regard, green synthesis using plant extract is the most promising approach for the facile synthesis of NPs.

Psidium guajava, also known as guava, is a member of the family Myrtaceae. *Psidium guava* is a medicinal plant, and its plant extract is rich in polyphenols (chlorogenic acid and guavin-B), flavonoids, carotenoids, and terpenoids.[21,22] The phytochemicals found in *Psidium guajava* serve as both reducing/oxidizing and capping agents in the synthesis of ZnO NPs.[21]

In the past several years, various coatings approaches have been reported to incorporate ZnO NPs on cotton fabric surfaces, including dip coating, layer-by-layer technique, and spray coating.[23] However, most of the methods require expensive equipment, high temperatures, and multistep procedures. Based on the methods documented in the literature, the pad-dry-cure method is considered one of the most suitable methods among the various coating approaches. The pad-dry-cure method has several advantages, such as simple, cost-effective, fast technique, lower consumption of electricity and chemicals, higher productivity, and uniform surface modification over a large area.[24] Thus, we were inspired to explore the use of the pad-dry-cure coating method and eco-friendly nanocomposite to develop mechanically and chemically stable and durable cotton fabrics with antibacterial and superhydrophobic functionalities. With this motivation, herein, we have synthesized ZnO NPs by treating *Psidium guajava* leaf extract with zinc acetate aqueous solution. Subsequently, the chitosan–zinc oxide nanocomposite (CS–ZnO) was synthesized and deposited onto the cotton fabric using the pad-dry-cure method. The prepared ZnO NPs, CS–ZnO, and CS–ZnO-coated cotton fabric (CS–ZnO CF) were characterized using various techniques, such as UV-visible (UV-Vis) spectroscopy, X-ray diffraction (XRD), Fourier transform infrared spectroscopy (FTIR), attenuated total reflectance-Fourier transform infrared (ATR-FTIR), scanning electron microscopy (SEM), energy-dispersive X-ray analysis (EDAX), and atomic force microscopy (AFM). Additionally, the mechanical properties of CS–ZnO CF and the uncoated cotton fabric (UCF) were investigated. The mechanical and washing durability of the prepared superhydrophobic fabric was assessed by abrasion and washing experiments. The disc diffusion method was employed to evaluate the antibacterial activity of the ZnO NPs, CS–ZnO, UCF, and CS–ZnO CF against *Staphylococcus aureus* (*S. aureus*) and *Escherichia coli* (*E. coli*) bacteria. Therefore, we consider this report to be a significant advancement toward the development of CS–ZnO nanocomposite-coated fabrics that exhibit promising potential for use as antibacterial and superhydrophobic textiles in hospital-related applications.

2. Experimental

2.1. Materials

Psidium guajava leaves were collected from the local area. Zinc acetate dihydrate ($Zn(CH_3COO)_2 \cdot 2H_2O$), sodium hydroxide (NaOH), chitosan (low molecular weight, degree of deacetylation 70–90%), and glacial acetic acid (CH_3COOH) of analytical grade were procured from Sigma-Aldrich Pvt., Ltd. India. Pristine cotton (100%) fabric with 148 ends per inch and 85 picks per inch, thickness of 0.2 mm, GSM 103 g m^{-2}, and density of 0.5 g cm^{-3} were procured from Dattajirao Kadam Technical Education (DKTE) Textile and Engineering Institute, Ichalkaranji, Maharashtra. All experiments were conducted using double-distilled water (DDW).

2.2. Bio-synthesis of ZnO NPs

ZnO NPs were synthesized using the bio-mediated co-precipitation method. In brief, the fresh *Psidium guajava* leaves were collected from the local area. The collected leaves were washed with DDW. The washed leaves were shade-dried for 10 days. To prepare the leaf extract, 30 g of finely cut dried leaves were added to 150 mL of DDW. Subsequently, the solution was boiled at 60 °C for 20 min. The obtained extract solution was allowed to cool to room temperature, and subsequently

filtered to eliminate the particulate matter. The obtained extract was stored in a refrigerator for subsequent use. After that, 10 mL of leaf extract was poured into 50 mL of 0.1 M $Zn(CH_3COO)_2 \cdot 2H_2O$ solution. The solution was stirred continuously for 2 h to obtain a white precipitate, which was eventually washed with DDW, followed by ethanol to remove the impurities. Furthermore, the precipitate was dried in an oven at 60 °C, followed by calcination at 500 °C for 2 h. The theoretical yield was 0.403 g, while the experimental yield was observed to be 0.352 g (87.34% yield).

2.3. Preparation of the CS–ZnO nanocomposite

To prepare the CS–ZnO nanocomposite, 1 g of chitosan was added to 100 mL of 2% (v/v) aqueous acetic acid solution (CH_3COOH) and stirred for 12 h at 60 °C. Subsequently, 2 g of biosynthesized ZnO NPs was added to the aforementioned solution, and it was continuously stirred at 60 °C for 2 h. Following that, 1 M sodium hydroxide (NaOH) was gradually added to the solution until it reached a pH of ~10. Finally, the resulting solution was sonicated for 1 h.

2.4. CS–ZnO nanocomposite-impregnated cotton fabric

Pristine cotton (100%) fabric with 148 ends per inch and 85 picks per inch was used for the application purpose. The prepared CS–ZnO solution was applied to the cotton fabric using the pad-dry-cure method. A cotton fabric cut to the size of 15×15 cm^2 was submerged in the CS–ZnO solution for 30 min. Subsequently, it was passed through a padding mangle (Universal Padding Mangle, R. B. Electronics Pvt. Ltd., India) operating at a speed of 15 m min^{-1} and a pressure of 1 kgf cm^{-2} to eliminate excess solution. This procedure was repeated three times to obtain an effective impregnation/coating of the nanocomposite onto the fabric surface (the obtained recovered CS–ZnO solution was filtered, and washed, and the dried powder was used for characterization). A wet pick of up of 90% was consistently maintained for all the treatments following the padding process, and the fabric was air-dried at 80 °C for 3 min and then cured for 2 min at 140 °C.

2.5. Characterization techniques

The UV-Vis spectra of the sample were recorded using a UV-visible spectrometer (Analytik Jena Specord 210 Plus). An X-ray diffractometer was used to characterize the crystal structure and phase formation of the sample (XRD-Bruker D8-Phaser, Cu $K\alpha_1$ radiation, $\lambda = 1.5406$ Å) in the diffraction angle range from 5° to 80°. Fourier transform infrared spectroscopy (FTIR-Bruker Alpha-100508 Spectrometer) was used to determine the functional groups present in the synthesized material from a wavenumber range of 400–4000 cm^{-1} (trace amount of sample in KBr pellets). Attenuated total reflectance-Fourier transform infrared (ATR-FTIR) spectra of UCF and CS–ZnO CF were recorded in the wavenumber range of 560–4000 cm^{-1} using Bruker, ALPHA, Germany. The morphological evolution and elemental composition of the materials were studied by scanning electron microscopy (SEM-JEOL, JSM-IT200) and energy-dispersive X-ray analysis (EDAX-JEOL, JSMIT200) with an accelerating voltage of 5–10 keV. Thermogravimetric analysis was performed using TGA, TA instrumentation, USA, SDT Q600 to evaluate the composition of ZnO and CS in CS–ZnO CF. The thermograms were recorded within the temperature range from 30 to 500 °C with a heating rate of 5 °C min^{-1} under air atmosphere (20 mL min^{-1}). An atomic force microscope (AFM, Park System Korea, NX10) was used to analyze the surface roughness of the sample. To determine the wettability of the sample, water contact angle (WCA) measurements were performed using the Holmarc contact meter model HO-IAD-CAM-01. A sessile drop method was employed to determine the $\theta°$ values. A 5 μL volume of DDW was positioned onto the fabric surface using a micro-syringe. The $\theta°$ was measured at four equidistant positions and the images were recorded at each position, with values subsequently averaged.

2.6. Durability test

The mechanical and washing durability of the as-prepared superhydrophobic fabric was evaluated by abrasion and washing experiments. In the abrasion experiment, the fabric was cut (38 mm circular diameter) and placed with the technical face down into a gold ring under a load of 200 g, maintaining a pressure of 9 kPa, and moving at a speed of 3 cm s^{-1} in one direction (Martindale Abrasion Tester, Mag Evolvics, Coimbatore). WCA was measured at an interval of 10 cycles. The impact of the abrasion cycles on the contact angle of the sample was investigated.

Studies on the wash durability of CS–ZnO CF were carried out with a washing fastness tester (DRS-3A-10) by (AATCC 61/2A-1996, AATCC 61-2006 test method). CS–ZnO CF was washed in a standard washing solution containing 2 g per L detergent. Each washing cycle was continued for 15 min at 40 °C. After washing (5, 10, 15, 20, 25 cycles), cotton fabrics were rinsed with DDW and subsequently dried at 50 °C for 6 h before conducting the WCA measurement.[25]

2.7. Mechanical properties

The textile engineering characterization, including analysis of the tensile strength and elongation at break, of UCF and CS–ZnO CF was performed using an Instron 5565 instrument (USA and Canada). The air permeability of UCF and CS–ZnO CF was assessed at room temperature with a pressure of 100 Pa using a Testex Air Permeability Tester.

2.8. Antibacterial activity

The disc diffusion method was used to assess the antibacterial activity of ZnO NPs, CS–ZnO, UCF, and CS–ZnO CF against *Escherichia coli* (*E. coli*-NCIM 2832) and *Staphylococcus aureus* (*S. aureus*-NCIM 2654). In this method, the test microorganisms were evenly spread onto the sterile nutrient agar plates, and the ZnO NPs (50 μg mL^{-1}), and circular-shaped 1 cm diameter discs of UCF and CS–ZnO CF were subsequently placed in Petri plates, which were incubated at 37 °C for 24 h. Then, the zone of inhibition was measured.

According to the standard AATCC100 method, UCF and CS–ZnO CF were cut into round pieces with a diameter of 1 cm. The

fabric samples were then dipped in bacterial cultures of *E. coli* and *S. aureus* and incubated at 37 °C for 24 h. Afterward, 0.1 mL of incubated culture was swabbed onto sterile media and incubated again at 37 °C for 24 h. The viable cell count method was utilized to determine the percentage of bacterial reduction using the following formula (eqn (1)),

$$\% \text{ bacterial reduction} = \frac{A - B}{A} \times 100 \quad (1)$$

where the initial number of cells is taken as A, and the final number of cells is taken as B.

3. Results and discussion

3.1. UV-visible spectroscopy

UV-visible spectroscopy was employed to investigate the synthesized ZnO NPs and CS–ZnO (Fig. 1a). The prepared ZnO NPs and CS–ZnO exhibited absorption peaks at 375 and 357 nm, respectively. Similar results were reported in earlier literature.[26,27] The UV-Vis spectra reveal that the absorption peak around 375 nm is the intrinsic band gap absorption of ZnO NPs. This is due to the electron transition from the valence band to the conduction band ($O_{2p} \rightarrow Zn_{3d}$).[28] Meanwhile, CS–ZnO exhibits an absorption peak at 357 nm. This absorption showed a blue shift, which is mainly due to the interaction with the chitosan. The band gap was evaluated using eqn (2), where λ_g is the wavelength of the absorption edge.

$$E_g = \frac{1240}{\lambda_g} \quad (2)$$

The ZnO NPs and CS–ZnO revealed a band gap of 3.30 and 3.47 eV, respectively, which was in agreement with an earlier report.[27,29] The observed blue shift denotes the decrease in the size of the particles and the increase in the band gap energy.[30]

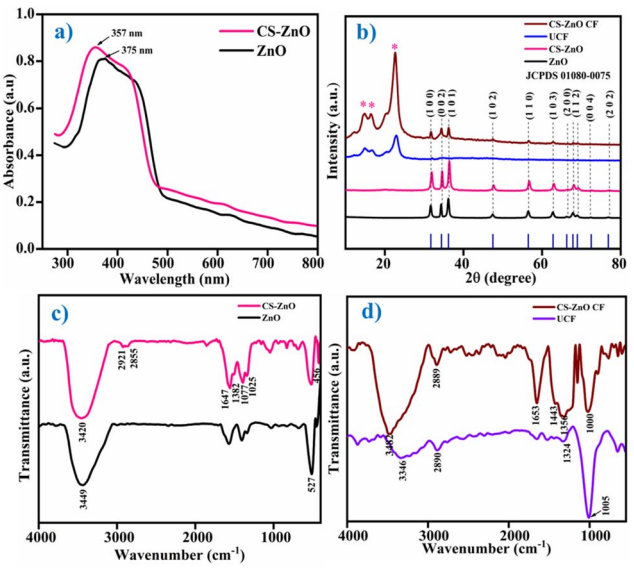

Fig. 1 (a) UV-visible spectra of ZnO and CS–ZnO. (b) XRD patterns of ZnO, CS–ZnO, UCF, and CS–ZnO CF. (c) FTIR spectra of ZnO and CS–ZnO. (d) ATR-FTIR spectra of UCF and CS–ZnO CF.

3.2. XRD analysis

Fig. 1b illustrates the XRD patterns of ZnO NPs, CS–ZnO, UCF, and CS–ZnO CF. The XRD pattern of ZnO NPs shows the diffraction peaks at $2\theta = 31.8$, 34.5, 36.3, 47.7, 56.8, 62.9, 66.5, 68.0, 72.5, and 76.9°, which were ascribed to the (100), (002), (101), (102), (110), (103), (200), (112), (004) and (202) planes of the ZnO crystal structure, respectively. The all-diffraction peaks were well indexed as hexagonal phases with the wurtzite crystal structure of ZnO NPs (JCPDS card no. 01080075). CS–ZnO indicates the presence of all peaks of ZnO NPs. However, a shift in two peaks at $2\theta = \sim31.92°$ (100) and $\sim36.40°$ (101) was observed.[31]

The additional peak noted in CS–ZnO (Fig. S1†) at $2\theta = 20.2°$ corresponds to the (200) plane due to chitosan, which exhibits the crystalline nature of chitosan.[32,33] These results reveal the successful synthesis of the CS–ZnO nanocomposite. In addition, the crystallite size of ZnO NPs and CS–ZnO was evaluated using Debye–Scherrer's formula (eqn (3))

$$D = \frac{0.9 \times \lambda}{\beta \cos \theta} \quad (3)$$

where D is the crystallite size in nm, λ is the X-ray wavelength (1.54 Å), β is the full-width-at-half-maximum (FWHM), and θ is the angle of diffraction. However, the average crystallite size was found to be 18.98 nm and 16.97 nm for ZnO NPs and CS–ZnO, respectively.[34] Furthermore, the XRD spectrum of UCF (marked with an asterisk) exhibits the diffraction peaks at $2\theta = 14.9$, 16.8 and 22.8°, which are indexed to the ($1\bar{1}0$), (110), and (200) crystal planes, respectively, of monolithic cellulose type I. This is in good agreement with the (JCPDS card no. 00-056-1717 and 00-0561718).[24] CS–ZnO CF showed diffraction peaks corresponding to cotton fabric and the CS–ZnO nanocomposite, supporting the fact that CS–ZnO was coated on the cotton fabric.

3.3. FTIR analysis

The FTIR spectra of ZnO NPs and CS–ZnO are presented in Fig. 1c. The FTIR spectrum of ZnO NPs exhibits the peaks at 3449 and 527 cm^{-1}, which could be attributed to the OH stretch and Zn–O bonding, respectively.[34] The FTIR spectrum of CS–ZnO exhibited peaks at 3420, 2921, 2855, 1647, 1382, 1077, and 1025 cm^{-1}, corresponding to the combined peaks of NH_2 and OH groups stretching, C–H stretching in CH_3, C–H stretching of CH_2, H-bonded amide I group of the combined vibrations of the C=O stretch and N–H deformation, CH_3 deformation, amine (C–N) stretching, and (C–O) stretching vibrations of chitosan, respectively.[34–36] Moreover, a peak at 456 cm^{-1} corresponding to Zn–O stretching was also observed.[10] This peak is observed to shift to a lower wavenumber as compared to that of the biosynthesized ZnO NPs, which indicates the formation of H-bonds between ZnO and chitosan. The decrease in the intensity of this peak with a new peak appearing at 456 cm^{-1} indicates the binding of ZnO NPs on chitosan, *i.e.*, the formation of

CS–ZnO.[32,36] The schematic structure of the CS–ZnO nanocomposite is depicted in Fig. S2.†

Moreover, an analysis of the functional groups in CS–ZnO CF was conducted *via* ATR-FTIR spectra and compared with UCF, as illustrated in Fig. 1d. UCF exhibited peaks at 3346, 2890, 1324 and 1005 cm^{-1}, which could be attributed to the OH stretching, C–H stretching, C–O bending, and C–O stretching vibrations in cellulose, respectively.[37] However, CS–ZnO CF endows the characteristic peaks at 3482, 2889, 1653, 1443, 1356, and 1000 cm^{-1}, corresponding to OH stretching (in cellulose), C–H stretching (in cellulose), C=O stretching (in chitosan), C–N stretching (in chitosan), and C–O stretching (in cellulose), respectively.[15,33,34] CS–ZnO CF shows the peaks of cotton fabric and CS–ZnO. A shift in some peaks is observed due to the interaction between the nanocomposite components and the cotton fabric.[34,37] The ATR-FTIR results support the coating of CS–ZnO on cotton fabric.

3.4. SEM and EDAX analysis

The surface morphology and elemental composition of UCF and CS–ZnO CF were examined using SEM and EDAX analysis, as illustrated in Fig. 2. The SEM images of UCF in Fig. 2a and b reveal a fiber with a smooth surface without any deposition. CS–ZnO CF (Fig. 2c and d) shows the CS–ZnO nanocomposite being uniformly coated on the fabric fiber surface, and the fiber surface subsequently becomes rough (see the high-magnification micrographs insets). Treatment with CS–ZnO causes an increase in the roughness of the cotton fabric surface, which is also supported by the AFM (given below).[38] Similar findings were documented in earlier literature.[39] These results demonstrate the homogenous distribution of the CS–ZnO nanocomposite all over the fabric surface and the subsequent surface roughness of the treated cotton, which is helpful for superhydrophobic properties.[40]

To confirm the coating of CS–ZnO on the cotton fabric, it was analyzed by EDAX analysis and compared with UCF, as shown in Fig. 2e and f. UCF (Fig. 2e) shows the presence of C (41.31%) and O (58.69%) elements. The carbon peak in the EDAX pattern originates from the cellulosic structure of the cotton fabric.[41] Conversely, CS–ZnO CF (Fig. 2f) exhibits the presence of C (9.67%), N (2.01%), Zn (64.15%), and O (24.17%) elements, supporting the deposition of ZnO NPs. The presence of other elements like N justifies its contribution due to the presence of chitosan in the CS–ZnO nanocomposite.[9,42] The EDAX spectra demonstrate that the CS–ZnO nanocomposite is successfully coated on the cotton fabric.

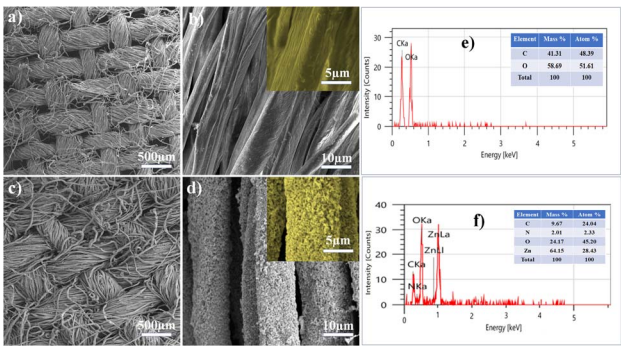

Fig. 2 SEM images of (a and b) UCF and (c and d) CS–ZnO CF. The insets show the magnified images. EDAX patterns of (e) UCF and (f) CS–ZnO CF.

3.5. TGA analysis

The amount of loading of CS and ZnO NPs on cotton fabric was assessed by employing TGA analysis. The TGA thermograms of UCF, ZnO CF, and CS–ZnO CF are depicted in Fig. S3.† The TGA thermogram of the UCF fabric shows the first weight loss below 100 °C, which is ascribed to the elimination of physically absorbed water. Further weight loss was observed at around 325 °C and 425 °C to 450 °C, which was attributed to the decomposition and oxidation of cellulose, revealing 100% weight loss. At higher temperatures above 500 °C, no additional weight loss was observed. By comparison, the ZnO CF fabrics showing an initial weight loss below 100 °C, which was attributed to the loss of water content. The second weight loss from 235 to 450 °C is due to the decomposition and oxidation of cellulose. However, at higher temperatures beyond 500 °C, no additional weight loss was observed due to the stability of the metal oxide (ZnO), which also indicates the ZnO loading on the cotton fabric. CS–ZnO CF was also studied, and exhibited an initial weight at around 100 °C due to the loss of surface adsorbed water. The second weight loss at 235–450 °C accounts for the combined loss due to the decomposition and oxidation of CS and cellulose of the fabric. As expected, at higher temperatures beyond 500 °C, no additional weight loss was noted, as only ZnO was the remnant. Interestingly, the TGA thermograms of ZnO CF and CS–ZnO CF showed total weight losses of 79.4%, and 82.5%, respectively. The difference in weight losses of 20.6% and 17.5% as compared to UCF corresponds to the amount of NPs of ZnO loaded on the cotton fabric for ZnO CF and CS–ZnO CF, respectively, as shown in Fig. S3.† Furthermore, the difference in the weight losses, *i.e.*, 20.6–17.5% = 3.1%, accounts for the CS loading. We believe that this would be the first report of estimating the CS content of the CS–ZnO composite using TGA.

3.6. AFM analysis

The formation of the superhydrophobic interface is influenced significantly by surface roughness. The surface roughness of CS–ZnO CF was examined by AFM and compared with that of UCF, which is presented in Fig. 3. UCF, as depicted in (Fig. 3a and c), displays the typical texture and relatively smooth surface with the root-mean-square (RMS) value of 42.6 nm. However, after coating of CS–ZnO on the cotton fabric, it exhibited an increase in surface roughness (Fig. 3b and d). Furthermore, the RMS value was augmented to 83.2 nm, which was higher than UCF. The RMS value was assessed as a measure of roughness, wherein the higher RMS values indicate increased surface roughness.[4] The CS–ZnO CF revealed distinctly rougher texture and substantial height variations, resembling mountain-shaped protrusions (Fig. 3b). The mountain-shaped protrusion is

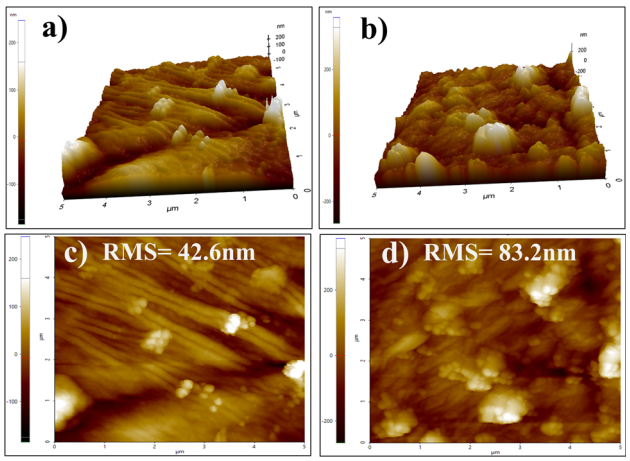

Fig. 3 AFM three-dimensional (3D) surface structures, and two-dimensional (2D) images of (a and c) UCF and (b and d) CS–ZnO CF, respectively.

thought to trap air within the pockets formed among the peaks, forming a stable air layer. This configuration creates a hydrophobic surface by reducing the contact area between water droplets and the fabric surface when water comes into contact with the fabric.[23,43] As a result, CS–ZnO CF exhibits good roughness, which is required to derive good super-hydrophobicity. Moreover, such superhydrophobic surfaces prevent the formation of bacterial biofilms and fabric contamination.[44]

3.7. Wettability

The wettability of UCF and CS–ZnO CF was examined by measuring the WCA, which is shown in Fig. 4. Fig. 4c shows that UCF was immediately wetted by a water droplet and the WCA (Fig. 4a) was close to 0°. This is because the water rapidly gets absorbed into the fabric in a few seconds. The outstanding hydrophilicity was attributed to the presence of abundant hydroxyl groups in cellulose.[2] On the contrary, CS–ZnO CF (Fig. 4b) shows a WCA of 153.15°, which confirms that the surface displays super-hydrophobicity (Fig. 4d). Theoretically, a surface with a WCA value greater than 150° can be termed as superhydrophobic.[43] According to the Zisman rule, the hydrophobic property could be increased when the surface possesses low surface energy.[4,43] Additionally, the Wenzel model proposes that the surface roughness enhances the hydrophobic characteristics.[43,45] As seen in the SEM images (Fig. 2d–f) and AFM (Fig. 3b and d), CS–ZnO CF possesses increased roughness and exhibits good superhydrophobic properties. Surfaces with greater hydrophobicity have a stronger antibacterial effect.[46] Particularly, superhydrophobic surfaces possess antibacterial and anti-adhesion properties because they have nano/microscale structures in addition to water-repellent properties, which restrict access to bacteria on the surface and inhibit the formation of bacterial biofilms.[44]

3.8. Durability test

In daily life, functional fabrics are required to demonstrate durability, particularly in terms of mechanical abrasion stress. In our study, the abrasion test of CS–ZnO CF was analyzed. As shown in Fig. 5a, the WCA value of CS–ZnO CF slightly decreases as the number of abrasion cycles increases. However, even after 50 abrasion cycles, CS–ZnO CF still maintained good super-hydrophobicity, revealing a WCA of 150.05°. Photographic images are presented in Fig. 5a, illustrating the water droplets on CS–ZnO CF both before and after 50 abrasion cycles. This suggests that the CS–ZnO coating exhibits remarkable mechanical durability and possesses excellent adhesion to cotton fabric. This is justified by the fact that even after the 50-cycles abrasion study, its super-hydrophobicity with a WCA of 150.05° was retained. Furthermore, the washing durability of CS–ZnO CF was evaluated and the WCA of CS–ZnO CF was measured (after intervals of five washing cycles), which is shown in Fig. 5b.

The photographic images of the water droplets on CS–ZnO CF (before and after 25 washing cycles) are shown in the inset of

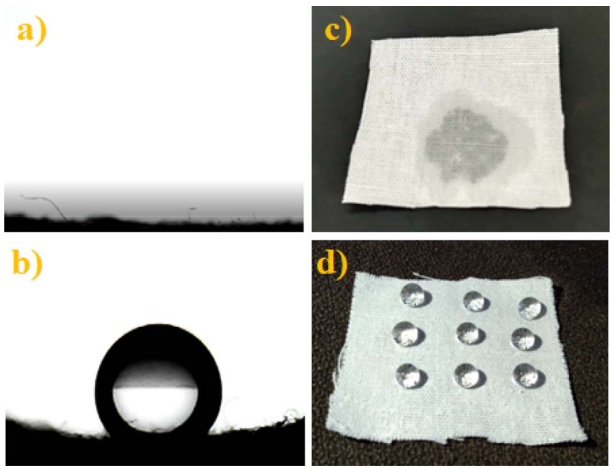

Fig. 4 Water contact angle (WCA) and photographic images of UCF (a and c) and CS–ZnO CF (b and d), respectively.

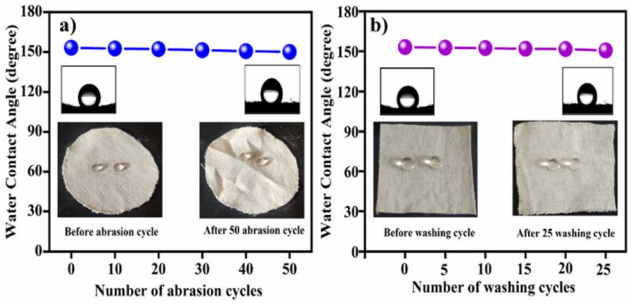

Fig. 5 (a) Variation in the WCA of CS–ZnO CF measured before and after the number of abrasion cycles (inset shows the representative photographic images of the water droplet on fabric before and after 50 abrasion cycles). (b) Variation in the WCA of CS–ZnO CF measured before and after the number of washing cycles (inset shows representative photographic images of the water droplet on fabric before and after 25 washing cycles).

Fig. 5b. It was observed that WCA slightly decreases with increasing number of washing cycles. However, it retained a WCA of 150.7° even after 25 washing cycles, indicating the excellent washing durability of the CS–ZnO superhydrophobic cotton textile.

3.9. Mechanical properties

Mechanical properties are among the primary concerns when evaluating the practical applications of a superhydrophobic coating material. To study the effectiveness of the coating material and the coating method, the mechanical properties (such as tensile strength and elongation at break, and air permeability) of CS–ZnO CF were investigated and compared with UCF, which are presented in Table 1.

The tensile strength and breaking at elongation of UCF and CS–ZnO CF are presented in Table 1. The results reveal that the tensile strength of CS–ZnO CF is slightly less compared with that of UCF. However, the breaking at elongation of CS–ZnO CF shows a significant increase, which is due to the CS–ZnO coating on cotton fabrics providing extra reinforcement. As a result, the experimental conditions, pad-dry-cure method, and coating of CS–ZnO did not affect the tensile property and structure of cotton fiber to a significant level. In addition, air permeability for UCF and CS–ZnO CF was also investigated. The air permeability of UCF was 88.06 $cm^3\ cm^{-2}\ s^{-1}$, whereas that for CS–ZnO CF was 53.97 $cm^3\ cm^{-2}\ s^{-1}$. It was observed that the air permeability of CS–ZnO CF was slightly less than that of UCF. This can be attributed to the deposition of the nanocomposite, which effectively closed the open interstices of the fabric, leading to a reduction in the fabric's air permeability.[47] It is interesting to note that this coating of natural material (chitosan) on cotton with a safe method involving a relatively low processing temperature ensures no or minimal alternations in the fabric properties. All these results indicate that there is little change in the fabric properties. Thus, it can be inferred that chitosan as a natural biopolymer has no negative effect on the physical properties of the finished fabric, and the pad-dry-cure method is a safe method for textile finishing.[48]

3.10. Antibacterial activity

The disc diffusion method was used to assess the antibacterial activity of ZnO NPs, CS–ZnO, UCF, and CS–ZnO CF against *S. aureus* and *E. coli* bacteria. The zone of inhibition (mm) of ZnO NPs, CS–ZnO, UCF, and CS–ZnO CF is shown in (Fig. 6, Table 2, and Fig. 7, Table 3).

The zone of inhibition of ZnO NPs against *S. aureus* and *E. coli* bacteria is illustrated in (Fig. 6a and b) and Table 2. The findings indicate that ZnO NPs exhibit greater antibacterial efficacy against *S. aureus* and *E. coli* bacteria. The structural difference in the cells of the bacteria is one of the possible reasons for the different sensitivity. Generally, the cell wall of Gram-negative bacteria (*E. coli*) is thick and has a more complex structure as compared to that of Gram-positive bacteria (*S. aureus*), making it less prone to the antibacterial action of ZnO NPs.[49,50] Similar results have been reported in earlier literature.[37,51] However, CS–ZnO has enhanced antibacterial activity as compared to ZnO (Fig. 6a and b, and Table 2). The enhanced antibacterial activity was attributed to the synergistic effect of chitosan and ZnO NPs. Furthermore, the smaller particle size contributes to a higher surface area-to-volume ratio than larger particles, which is thought to be responsible for the improved biocidal activity of the nanocomposite.[52] The abovementioned

Table 1 Mechanical properties of UCF and CS–ZnO CF

Specimen	Tensile strength (N)	Elongation (mm)	Air permeability ($cm^3\ cm^{-2}\ s^{-1}$)
UCF	431.29	19.30	88.06
CS–ZnO CF	396.27	21.20	53.97

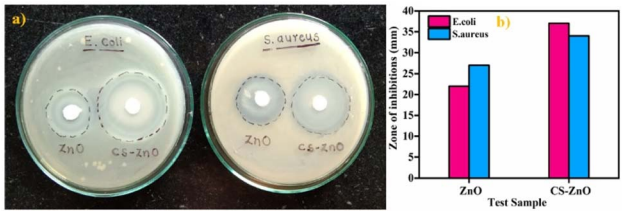

Fig. 6 (a) and (b) Antibacterial activity of the ZnO NPs and CS–ZnO nanocomposite against *E. coli* and *S. aureus*.

Table 2 Zone of inhibition (mm) of the ZnO NPs and CS–ZnO nanocomposite

	Zone of inhibition (mm)	
Test sample	*E. coli*	*S. aureus*
ZnO	22	27
CS–ZnO	37	34

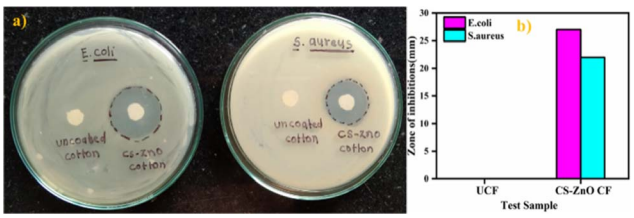

Fig. 7 (a) and (b) Antibacterial activity of UCF and CS–ZnO CF against *E. coli* and *S. aureus*.

Table 3 Antibacterial activity of UCF and CS–ZnO CF, as per zone of inhibition (mm) and bacterial reduction percentage, employing the AATCC100 standard test

	Zone of inhibition (mm)		Bacterial reduction percentage (%)	
Test sample	*E. coli*	*S. aureus*	*E. coli*	*S. aureus*
UCF	00	00	00	00
CS–ZnO CF	27	22	83 ± 1.6	75.6 ± 1.1

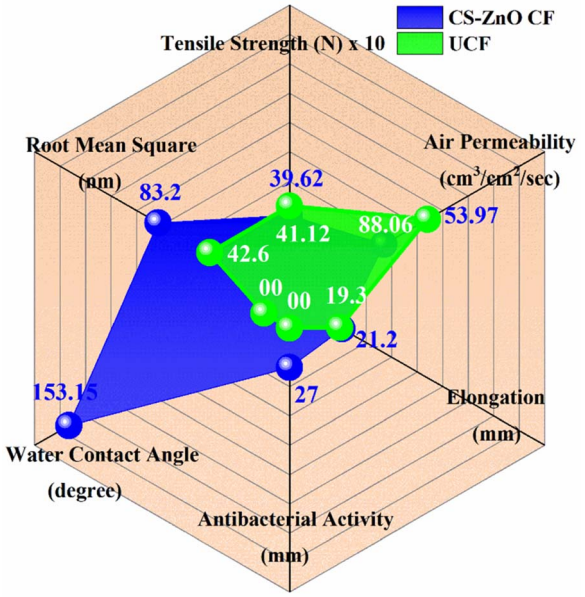

Fig. 8 Radar plot comparing the antibacterial, mechanical, physico-chemical, and superhydrophobic properties of UCF (green curve) and CS–ZnO CF (blue curve).

results corroborate the UV and XRD results of the CS–ZnO nanocomposite.

Based on the results obtained in Table 2, CS–ZnO exhibited greater antibacterial activity against Gram-negative bacteria (*E. coli*) as compared to Gram-positive bacteria (*S. aureus*). This can be attributed to the nanocomposite's permeability into the bacterial cell wall, along with the attraction between the negatively charged bacteria and positively charged CS–ZnO nanocomposite, which contributes the higher bacterial inhibition.[9,27,34,53] As shown in Fig. 7a and Table 3, CS–ZnO CF shows a remarkable zone of inhibition against *E. coli* and *S. aureus*, whereas UCF did not show a zone of inhibition. This indicates that CS–ZnO CF exhibits good antibacterial activity towards bacterial pathogens.

The percentage reduction of UCF and CS–ZnO CF against *E. coli* and *S. aureus* is indicated in Table 3. It was observed that CS–ZnO CF shows higher antibacterial efficiency in both *E. coli* (83%) and *S. aureus* (75%). Conversely, UCF does not exhibit any bacterial reduction.

Overall, the results reveal that CS–ZnO CF shows good antibacterial and superhydrophobic properties as compared to UCF, which is presented in Fig. 8 in the form of a radar chart.

4. Conclusion

In this study, ZnO NPs were synthesized by a simple, inexpensive, green approach utilizing *Psidium guajava* leaf extract and zinc acetate. These ZnO NPs were combined with the chitosan solution to form the CS–ZnO nanocomposite. The UV-visible study confirmed the successful synthesis of ZnO and CS–ZnO nanocomposite. The XRD analysis revealed the hexagonal phase with the wurtzite crystal structure of ZnO NPs. The functional groups present in ZnO, CS–ZnO, and CS–ZnO CF were confirmed using FTIR analysis. SEM images of CS–ZnO CF depicted the distribution of CS–ZnO on the cotton fabric and the subsequent surface roughness. The EDAX analysis confirmed the existence of C, N, Zn, and O elements. The AFM study revealed that after the coating of CS–ZnO, an increase in the surface roughness (RMS value is 83.2 nm) was noted. As a result, CS–ZnO CF exhibited good super-hydrophobicity with a WCA of 153.15°. CS–ZnO CF displayed good hydrophobicity with a WCA of over 150° even after the 25 washing and 50 abrasion cycles. More importantly, CS–ZnO CF still retained good superhydrophobic properties after multiple washing cycles. In addition, the prepared ZnO NPs, CS–ZnO, and CS–ZnO CF showed significant antibacterial activity against *E. coli* and *S. aureus*. Overall, the findings indicate that the synthesis and the coating method are facile, time-saving, inexpensive, and scalable processes for large-scale production. Thus, our approach to producing multifunctional textiles that exhibit effective antibacterial properties and maintain durable superhydrophobic fabric could be valuable for the development of promising and protective clothing, particularly in moist and unsanitary environments.

Data availability

The data will be available from the corresponding author upon reasonable request.

Author contributions

K. S. Kachare: conceptualization of the project, conducting the experiments, following the investigation, methodology, data curation, interpretation, and writing the manuscript draft. S. S. Shendage: data curation, review, and editing. S. B. Vhanbatte: mechanical properties study, data curation, and review of the article. F. D. Mai: antibacterial study, data curation, writing, review & editing. A. V. Ghule: conceptualization of the project, planning of the experiments, guidelines for execution of the project, following the investigation, methodology, data curation, interpretation, supervision, validation, drafting of the manuscript, review and editing the draft.

Conflicts of interest

There are no conflicts to declare.

Acknowledgements

The author Kranti S. Kachare is thankful to Chhatrapati Shahu Maharaj Research, Training and Human Development Institute (SARTHI), Pune, Government of Maharashtra, India 411004, for the financial support in the form of Chhatrapati Shahu Maharaj National Research Fellowship-2021 (CSMNRF-2021), (CIN-U74999PN2018NPL177394). We are thankful to the Department of Chemistry, Shivaji University, Kolhapur for providing the research facilities. We are thankful to Shivaji University Group for Advanced Research "SUGAR" for helpful discussion.

References

1 N. Karim, S. Afroj, K. Lloyd, L. C. Oaten, D. V. Andreeva, C. Carr, A. D. Farmery, I. D. Kim and K. S. Novoselov, *ACS Nano*, 2020, **14**, 12313–12340.
2 M. Shaban, F. Mohamed and S. Abdallah, *Sci. Rep.*, 2018, **8**, 1–15.
3 N. Ghasemi and J. Seyfi, *Cellulose*, 2018, **25**, 4211–4222.
4 J. Chen, L. Yuan, C. Shi, C. Wu, Z. Long, H. Qiao, K. Wang and Q. H. Fan, *ACS Appl. Mater. Interfaces*, 2021, **13**, 18142–18151.
5 M. Raeisi, Y. Kazerouni, A. Mohammadi, M. Hashemi and I. Hejazi, *Int. J. Biol. Macromol.*, 2021, **171**, 158–165.
6 Y. Iqbal, I. Ahmed, M. Faisal, S. Ali, S. Chatha, M. Zubair and A. Ullah, *Carbohydr. Polym.*, 2023, **321**, 121318.
7 C. Liao, Y. Li, M. Gao, W. Chai, X. Su and Z. Zheng, *Colloids Surf., A*, 2023, **657**, 130586.
8 M. Markiewicz, J. Kumirska, I. Lynch, M. Matzke, J. Köser, S. Bemowsky, D. Docter, R. Stauber, D. Westmeier and S. Stolte, *Green Chem.*, 2018, **20**, 4133–4168.
9 D. Bharathi, R. Ranjith Kumar, B. Chandrashekhar and V. Bhuvaneshwari, *Int. J. Biol. Macromol.*, 2019, **129**, 989–996.
10 G. Madhan, A. A. Begam, L. V. Varsha, R. Ranjithkumar and D. Bharathi, *Int. J. Biol. Macromol.*, 2021, **190**, 259–269.
11 J. Kwiczak-Yiğitbaşi, Ö. Laçin, M. Demir, R. E. Ahan, U. Ö. Ş. Şeker and B. Baytekin, *Green Chem.*, 2020, **22**, 455–464.
12 Y. Iqbal, I. Ahmed, M. F. Irfan, S. A. S. Chatha, M. Zubair and A. Ullah, *Carbohydr. Polym.*, 2023, **321**, 121318.
13 C. Chen, X. Yang, S. J. Li, C. Zhang, Y. N. Ma, Y. X. Ma, P. Gao, S. Z. Gao and X. J. Huang, *Green Chem.*, 2021, **23**, 1794–1804.
14 M. Shahid, S. Maiti, R. V. Adivarekar and S. Liu, *Mater. Today Chem.*, 2022, **24**, 100940.
15 K. Bharathi Yazhini and H. Gurumallesh Prabu, *RSC Adv.*, 2015, **5**, 49062–49069.
16 M. E. El-Naggar, S. Shaarawy and A. A. Hebeish, *Carbohydr. Polym.*, 2018, **181**, 307–316.
17 I. Perelshtein, G. Applerot, N. Perkas, E. Wehrschetz-Sigl, A. Hasmann, G. M. Guebitz and A. Gedanken, *ACS Appl. Mater. Interfaces*, 2009, **1**, 361–366.
18 V. Bhandari, S. Jose, P. Badanayak, A. Sankaran and V. Anandan, *Ind. Eng. Chem. Res.*, 2021, **1**, 86–101.
19 M. Nasrullah, F. Z. Gul, S. Hanif, A. Mannan, S. Naz, J. S. Ali and M. Zia, *ACS Omega*, 2020, **5**, 5739–5747.
20 N. Bala, S. Saha, M. Chakraborty, M. Maiti, S. Das, R. Basu and P. Nandy, *RSC Adv.*, 2015, **5**, 4993–5003.
21 R. Saha, K. Subramani, S. A. K. Petchi Muthu Raju, S. Rangaraj and R. Venkatachalam, *Prog. Org. Coat.*, 2018, **124**, 80–91.
22 M. Rehan, O. A. Ahmed-Farid, S. R. Ibrahim, A. A. Hassan, A. M. Abdelrazek, N. I. M. Khafaga and T. A. Khattab, *ACS Sustain. Chem. Eng.*, 2019, **7**, 18612–18623.
23 S. Xiaojing, L. Hongqiang, L. Xuejun, *et al.*, *ACS Appl. Mater. Interfaces*, 2017, **9**, 28089–28099.
24 D. K. Subbiah, A. Das, J. Bosco and B. Rayappan, *Appl. Surf. Sci.*, 2020, **541**, 148378.
25 Y. Cheng, T. Zhu, S. Li, J. Huang, J. Mao, H. Yang, S. Gao, C. Zhong and Y. Lai, *Chem. Eng. J.*, 2018, **355**, 290–298.
26 N. A. A. Yusof, N. M. Zain and N. Pauzi, *Int. J. Biol. Macromol.*, 2019, **124**, 1132–1136.
27 S. H. S. Dananjaya, R. S. Kumar, M. Yang, C. Nikapitiya, J. Lee and M. De Zoysa, *Int. J. Biol. Macromol.*, 2018, **108**, 1281–1288.
28 R. A. Krishnan, O. Mhatre, J. Sheth, S. Prabhu, R. Jain and P. Dandekar, *J. Polym. Res.*, 2020, **27**, 206.
29 K. Mageshwari, T. G. Kim and J. Park, *J. Mater. Sci.: Mater. Electron.*, 2016, **27**, 4093–4097.
30 T. Abiraman, G. Kavitha, R. Rengasamy and S. Balasubramanian, *RSC Adv.*, 2016, **6**, 69206–69217.
31 K. Rasool, G. Nasrallah, N. Yones, R. Pandey, *et al.*, *ACS Sustain. Chem. Eng.*, 2018, **6**, 3896–3906.
32 M. Türemen, A. Demir and Y. Gokce, *Mater. Chem. Phys.*, 2021, **268**, 124736.
33 S. Preethi, K. Abarna, M. Nithyasri, P. Kishore, K. Deepika, R. Ranjithkumar, V. Bhuvaneshwari and D. Bharathi, *Int. J. Biol. Macromol.*, 2020, **164**, 2779–2787.
34 T. Revathi and S. Thambidurai, *Adv. Powder Technol.*, 2018, **29**, 1445–1454.
35 P. Mujeeb Rahman, K. Muraleedaran and V. M. A. Mujeeb, *Int. J. Biol. Macromol.*, 2015, **77**, 266–272.
36 A. M. Díez-Pascual and A. L. Díez-Vicente, *Biomacromolecules*, 2015, **16**, 2631–2644.
37 M. Hasanin, E. M. Swielam, N. A. Atwa and M. M. Agwa, *Int. J. Biol. Macromol.*, 2022, **197**, 121–130.
38 W. Cheng, W. Liu, P. Wang, M. Zhou, L. Cui, Q. Wang and Y. Yu, *Int. J. Biol. Macromol.*, 2022, **213**, 96–109.
39 Z. Ye, S. Li, S. Zhao, L. Deng, J. Zhang and A. Dong, *Chem. Eng. J.*, 2020, **373**, 127680.
40 E. K. Sam, D. K. Sam, X. Lv and B. Liu, *Chem. Eng. J.*, 2019, **373**, 531–546.
41 S. Ghayempour and M. Montazer, *Ultrason. Sonochem.*, 2017, **34**, 458–465.
42 G. Asgari-Targhi, A. Iranbakhsh, Z. Oraghi Ardebili and A. Hatami Tooski, *Int. J. Biol. Macromol.*, 2021, **189**, 170–182.
43 V. Ha, T. Thi, B. Lee and C. Ngo, *J. Taiwan Inst. Chem. Eng.*, 2017, **71**, 527–536.
44 S. A. Jalil, M. Akram, J. A. Bhat, J. Hayes and S. C. Singh, *Appl. Surf. Sci.*, 2020, **506**, 144952.
45 V. Pandiyarasan, S. Suhasini, J. Archana, M. Navaneethan, A. Majumdar, Y. Hayakawa and H. Ikeda, *Appl. Surf. Sci.*, 2017, **418**, 352–361.
46 J. Kim, S. H. Kang, Y. Choi, W. Lee, N. Kim, M. Tanaka, S. H. Kang and J. Choi, *Sci. Rep.*, 2023, **13**, 1–11.
47 A. Javed, M. Azeem, J. Wiener, M. Thukkaram, J. Saskova and T. Mansoor, *Fibers Polym.*, 2021, **22**, 77–86.
48 S. Roy, K. Goh, C. Verma, B. D. Ghosh, K. Sharma and P. K. Maji, *ACS Sustain. Chem. Eng.*, 2022, **10**, 4694–4704.
49 G. Nascimento and T. C. Daboit, *J. Cleaner Prod.*, 2019, **247**, 119085.

50 K. Lefatshe, C. M. Muiva and L. P. Kebaabetswe, *Carbohydr. Polym.*, 2017, **164**, 301–318.
51 S. Anitha, B. Brabu, D. J. Thiruvadigal, C. Gopalakrishnan and T. S. Natarajan, *Carbohydr. Polym.*, 2012, **87**, 1065–1072.
52 M. Karpuraranjith and S. Thambidurai, *Int. J. Biol. Macromol.*, 2017, **104**, 1753–1761.
53 P. M. Rahman, V. M. A. Mujeeb, K. Muraleedharan and S. K. Thomas, *Arabian J. Chem.*, 2016, **11**, 120–127.